RSC Advances

PAPER

View Article Online
View Journal | View Issue

Cite this: *RSC Adv.*, 2017, **7**, 44001

Structural characterization and electrochemical performance of macroporous graphite-like C_3N_3 prepared by the Wurtz reaction and heat treatment†

Hao Yin,[a] Qixun Guo,[a]* Dingzeng He,[a] Juntao Li*[a] and Shigang Sun[ab]

Macroporous graphite-like C_3N_3 (g-C_3N_3) with s-triazine rings as building blocks was synthesized by the Wurtz reaction of $C_3N_3Cl_3$ with sodium in autoclaves. The structure and electrochemical performance as a lithium ion battery anode of the obtained samples were then investigated. Structural characterization results reveal that the as-prepared samples show characteristic 002 basal plane diffractions and s-triazine rings structures with an N/C atomic ratio of about 1 : 1, indicating that the theoretical g-C_3N_3 has been successfully prepared. It was found that the heat treatment can help improve the initial coulombic efficiency and reversible capacity due to the decrease of the nitrogen content and the partial degradation and rearrangement of triazine rings. When used as an anode for Li-ion batteries, the g-C_3N_3 formed by heat treatment up to 600 °C exhibits a relatively good reversible capability and cycling stability (197.8 mA h g^{-1} at 100 mA g^{-1}), with measurements superior to those of reported bulk g-C_3N_4 and other graphite-like carbon nitride analogues.

Received 13th July 2017
Accepted 5th September 2017

DOI: 10.1039/c7ra07707f

rsc.li/rsc-advances

1. Introduction

Nowadays, increasing energy demands along with the depletion of conventional fossil fuel resources have greatly promoted the development of alternative energy conversion and storage systems. Lithium-ion batteries (LIBs) have become the predominant battery technology since their first commercialization in the 1990s and show significant potential for applications in electric vehicles (EVs) due to their characteristics of high-energy density, long cycling life and environmental friendliness.[1–4] In the last several decades, graphite plays a dominant role as the anode material in commercial lithium-ion batteries because of its good electrochemical performance, mechanical stability and low cost.[1,2,4]

However, low theoretical capacity (372 mA h g^{-1}), limited cycling life and poor rate performance of graphite significantly constrain the further development of LIBs.[4] Therefore, developing anode materials to replace graphite has become a research hotspot in recent years. Among the available anode materials, nitrogen rich porous carbon materials show great promise as alternative anode materials in LIBs. It has been found that the capacity of carbon materials can be increased by chemical doping heteroatoms, especially nitrogen atoms.[5–7] The reason of the enhancement is associated with the kinds of nitrogen containing groups, such as pyridinic nitrogen and graphitic nitrogen.[7,8] Liu *et al.* have carried out a great many research works on carbon materials and nitrogen doped materials.[9–11] Cheng *et al.* prepared the N-doped graphene electrodes with a high capacity of 1043 mA h g^{-1} at a current density of 50 mA g^{-1}, much improved reversible capacity and cycle performance compared with undoped graphene.[5] Wang *et al.* prepared covalently coupled hybrid of graphitic carbon nitride with graphene with a capacity of 1525 mA h g^{-1} at a current density of 100 mA g^{-1}.[1] It is known to all that the pyridinic N atoms are of avail to capacity enhancement by virtue of the stronger electro-negativity of nitrogen when compared to that of carbon.[1,7]

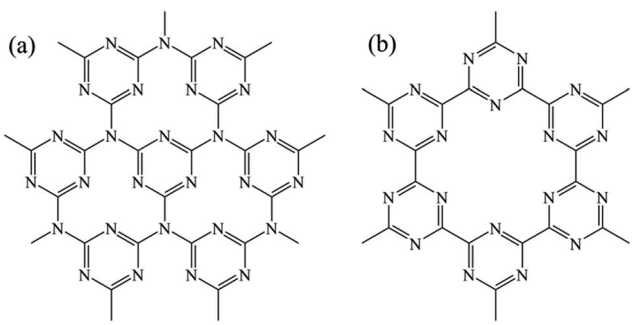

Fig. 1 The molecular structural schematic diagram of g-C_3N_4 (a) and g-C_3N_3 (b).

[a]*College of Energy, Xiamen University, Xiamen 361005, P. R. China. E-mail: qxguo@xmu.edu.cn; jtli@xmu.edu.cn; Tel: +86-592-5952737*

[b]*State Key Lab of Physical Chemistry of Solid Surface, College of Chemistry and Chemical Engineering, Xiamen University, Xiamen 361005, P. R. China*

† Electronic supplementary information (ESI) available. See DOI: 10.1039/c7ra07707f

The nitrogen rich porous carbon materials with 2D layered structure such as g-C_3N_4 and g-C_3N_3 (see Fig. 1), combining the advantages of graphite and nitrogen doping, will surely exhibit a higher capacity than pure graphite. Thereinto, g-C_3N_4 as anode materials has awaked much interest during last several years. Wu *et al.* performed a theoretical study showing that g-C_3N_4 has a capacity of 524 mA h g^{-1} corresponding to $Li_2C_3N_4$.[12] However, experimental studies have shown that a large capacity drop from over 130 mA h g^{-1} to only around 10 mA h g^{-1} in the first cycle.[8] Then Hankel *et al.* adopted DFT calculations and presented that Li^+ interacts strongly with pyridinic nitrogen, due to the high adsorption energy, causing a large irreversible capacity. Meanwhile, the existence of graphitic nitrogen is the weak point of the structure, making it unstable under high Li^+ loading.[7]

While for g-C_3N_3 or g-CN, without any graphitic nitrogen, has six pyridinic nitrogens per unit cell (see Fig. 1(b)) which should be more stable and better conductivity than g-C_3N_4 during high lithiation. Sheng *et al.* calculated the g-C_3N_3 has a band gap of around 1.5–1.6 eV.[13] Guo *et al.* and Cao *et al.* had synthesized the g-C_3N_3 and showed its self-assembly into nanotube bundles, aligned nanoribbons and microspheres, respectively.[14,15] Hankel *et al.* performed a theoretical study showing that g-C_3N_3 has a capacity of 813 mA h g^{-1} corresponding to LiCN while the layer retains its integrity with some distortion but not very much, indicating the g-C_3N_3 could be a proper candidate anode material.[16]

Herein, the theoretic g-C_3N_3 was synthesized based on the Guo's method[14] with some changes of reactants, reaction temperature, and autoclaves. The reaction scheme can be formulated as follows:

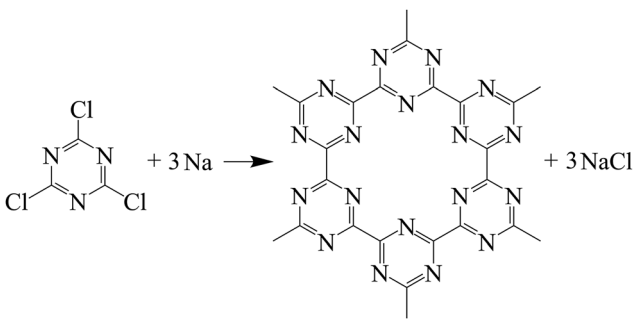

Then the synthesized g-C_3N_3 was used as anode material for LIBs. To the best of our knowledge, this is the first time that the electrochemical performance of g-C_3N_3 as anode material has been experimentally studied. Moreover, during the electrochemical characterization, it was found that the sample with further heat treatment at 600 °C (CN-480-600) delivered a better electrochemical performance than the pristine CN-480. And we preliminarily investigated the influence of heat treatment on the structure, composition, and electrochemical performance of the synthesized carbon nitride.

2. Experimental section

2.1. Synthesis of g-C_3N_3

In a typical experiment, 20 mmol $C_3N_3Cl_3$ (1,3,5-trichlorotriazine, Sigma-Aldrich) and 60 mmol sodium were placed into a 40 ml Al_2O_3 crucible with a plane lid in the glovebox before together transferred into stainless steel lined stainless steel autoclaves with 100 ml capacity. The sealed autoclave was heated from room temperature to 380 °C and 480 °C respectively with a speed of about 5 °C min^{-1}, and then kept at corresponding temperatures for 12 h, finally cooled to room temperature in the furnace naturally. The obtained samples were grinded carefully before sequentially washed with methylbenzene, ethanol, and distilled water for several times to remove residual impurities such as NaCl and unreacted raw materials, and then dried in a vacuum at 60 °C for several hours. Finally, the two kinds of dark black powders were obtained for characterization. The synthesized products were denoted as CN-380 and CN-480 according to the two degrees of the reaction temperatures. The yields of CN-380 and CN-480 were ~0.55 g and 0.90 g, respectively.

In addition, 0.30 g CN-480 was placed in a tube furnace and heated at 500 °C and 600 °C respectively for 30 min under a continuous Ar gas with a flow rate of 50 ml min^{-1}. The heat treated sample was denoted as CN-480-500 and CN-480-600, respectively. The yields of CN-480-500 and CN-480-600 were ~0.24 g and ~0.16 g, respectively.

2.2. Characterization

X-ray diffraction (XRD) measurements were tested using a Rigaku Ultima IV X-ray diffraction system with Cu radiation at 40 kV, 40 mA. FT-IR spectra were recorded with a Nicolet is50 Fourier transform infrared spectrometer, in transmission mode in a KBr pellet. Bulk elemental analysis (from C–H–N combustion) was taken on an Elementar Vario EL-III elemental analyzer. Thermal analysis was carried out on a NETZSCH STA 449F5 in nitrogen with an Al_2O_3 crucible in the temperature range of 35–1400 °C with a heating rate of 5 °C min^{-1}. X-ray photoelectron spectroscopy (XPS) measurements were performed using an ESCALAB 250Xi XPS System with a monochromatized Al Kα X-ray source (200 W, pass energy = 30 eV). FE-SEM images of synthesized samples were recorded on a ZEISS SUPRA 55 SAPPHIRE field emission scanning electron microscope. The surface areas of the as-synthesized samples were measured by the Brunauer–Emmett–Teller (BET) method using nitrogen adsorption and desorption isotherms on a Micromeritics ASAP 2020. The pore size distribution plots were obtained by the Barrett–Joyner–Halenda (BJH) method.

2.3. Electrochemical characterization

Electrodes were fabricated by using a conventional coating method. A slurry, consisting of the as-prepared active material (80 wt%), acetylene black (10 wt%) and polyvinylidene fluoride (10 wt%) in *N*-methyl-2-pyrrolidone, was uniformly spread onto a Cu foil. The as-prepared electrodes were dried at 110 °C for 12 h in a vacuum oven. In an argon-filled glove box, CR2025-type coin cells were assembled using lithium metal as the counter electrode, Celgard 2300 membrane as the separator and LiPF6 (1 M) in ethylene carbonate (EC)/dimethyl carbonate (DMC) (1 : 1 vol) as the electrolyte. Cyclic voltammograms (CVs) were collected by using an electrochemical workstation (CHI660E) at

a scan rate of 0.2 mV s^{-1}. Galvanostatic charge–discharge tests were performed by using Land (CT2001A) between 0.01 and 3.00 V (*versus* Li^+/Li). The calculated specific capacities were based on the weight of active materials and the typical loading of the active material on the Cu foil is about 1.3 ± 0.05 mg cm^{-2}.

3. Results and discussions

Fig. 2 shows the XRD patterns of the synthesized samples in different temperatures. The XRD patterns of CN-380, CN-480, CN-480-500 and CN-480-600 are characterized by a relatively strong reflection centred at about 26.4°, 27.1°, 26.7° and 26.7° with a *d* spacing of 3.37 Å, 3.29 Å, 3.34 Å and 3.34 Å, respectively. The four broad peaks, though slightly different in position, are all very similar to the characteristic peak of the 002 basal plane diffractions in graphite (d = 3.354 Å), nano-sized g-C_3N_4 (d = 3.25 Å)[17] and g-$CN_{0.96}$ ($d = 3.20 \pm 0.01$ Å),[14] indicating the major structure orderings of the two samples are related to the structure of graphite. Meanwhile, the peak of CN-480 shifts from 26.4° to 27.1° with a decrease in the interlayer stacking distance from 3.37 Å to 3.29 Å suggests the degree of condensation of synthesized carbon nitride will increase at higher reaction temperature.[18,19] On the other side, the FWHM (Full Width at Half Maximum) of 002 basal plane diffractions peak in CN-380 patterns (~8.3°) is larger than that in CN-480 patterns (~5.6°), suggesting the better crystallization of sample CN-480. After heat treatment to 600 °C, the FWHM of 002 basal plane diffractions peak becomes broader (~7.1°) and shifts from 27.1° to 26.7° which can be related to the partial degradation of the ordered interlayer stacking structure. Among them, the pattern of CN-480-500 is similar to that of CN-480-600 with just a narrower FWHM (~6.8°).

There are not any diffraction peaks of metal oxides and NaCl, indicating that the stainless steel has not been involved in the reaction and the samples have been washed extremely clean as well.

FTIR spectra of the synthesized samples are shown in Fig. 3. The FTIR spectra of the samples show the features very similar to those observed earlier by Guo,[14] Xu[17] and Zhang.[20] For the sample CN-380, a group of multiple bands is shown at about 1200–1600 cm^{-1} and about 800 cm^{-1}, typically indicating s-triazine rings vibration.[14,21,22] The bands at about 2169 cm^{-1} characterizes the cyano group (–N=C=N– or –C≡N) stretching, suggesting fracture of a small amount of triazine rings.[14,20,23] In addition, the peak observed at about 3405 cm^{-1} can be associated with O–H.[22,24] The position of bands of the sample CN-480, CN-480-500 and CN-480-600 are in consistent with that of the sample CN-380, indicating the s-triazine ring structure has also been successfully prepared at 480 °C. However, elevating reaction temperature (compare CN-380 with CN-480) causes a decrease of transmittance of the cyano group stretching at about 2169 cm^{-1}, suggesting that reaction temperature increasing may lead to the partial rupture of s-triazine rings structure. Whereas, as the band at about 1420 cm^{-1} is generally attributed to the C=N stretching.[22,25] Less transmittance of CN-480 than CN-380 at about 1420 cm^{-1} indicates the higher crystallinity of CN-480, which is in good agreement with the results of XRD.

To better understand the composition of synthesized samples, bulk elemental analysis has been carried out and the C–H–N combustion results of synthesized samples are shown in Table 1. To begin with, it should be note that a small amount of hydrogen content shows in the C–H–N combustion results. Since there is no any hydrogen source involved in the reaction, the detected hydrogen content can be attributed to the absorbed moisture and is excluded in the Table 1. The N/C ratio of the sample CN-480 are similar to the ratio of ideal g-C_3N_3. With the increasing of reaction temperature, the value of N/C mole ratio decreases a little but still approaches 1, suggesting a small amount of N atom loss when reaction temperature increases. Also, the N/C ratio reduces to about 0.84 after heat treatment confirming that the heat treatment leads to the removal of N element. By combining with the yields after heat treatment, C

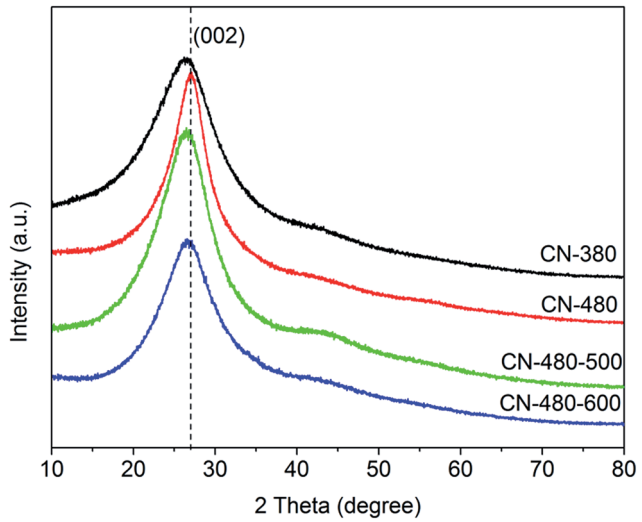

Fig. 2 XRD patterns of the synthesized samples.

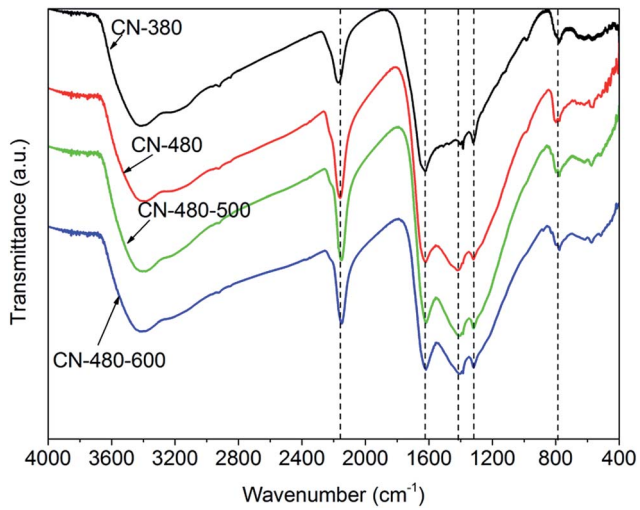

Fig. 3 FTIR spectra of the synthesized samples.

Table 1 Elemental analysis of synthesized samples with different heat treatment temperature

Samples	Bulk analysis (wt%) C	N	Total wt%	Empirical formula
CN-380	34.37	38.55	72.92	$CN_{0.96}$
CN-480	36.67	40.03	76.70	$CN_{0.94}$
CN-480-500	37.09	39.38	76.47	$CN_{0.91}$
CN-480-600	36.54	35.84	72.38	$CN_{0.84}$

atoms should also be removed in addition to N atoms during heat treatment. Based on the N/C ratio, it can be concluded that the loss of N atoms is greater than that of C atoms. The total mass of C–H–N in the treated samples is less than 100% and the other untested elements could be the oxygen which may enter into the autoclaves during the weighing process or moisture in the test samples.

From the TGA curves (Fig. 4), it is clearly shown that about 8% of mass loss at temperature below 200 °C, which can be attributed to removing the absorbed water. Due to the CN-480 is prepared at 480 °C, its structure can maintain stable between 200–500 °C. The huge mass loss at 500–1000 °C may result from the rupture of s-triazine rings structure and the removing of C, N atoms. A bulge between 800 °C and 1000 °C may be ascribed to partial graphitization. Originally, we set 600 °C as a proper heat treatment temperature based on the TGA curves. The samples at treatment temperature above 600 °C such as 700 °C and 800 °C are degraded too much that it is less meaningful and it is hard to examine the electrochemical performance. In this regard, 500 °C and 600 °C are chosen to be two heat treatment temperatures.

Besides, due to the superior electrochemical performance of CN-480-600 which will be shown in the following part of this manuscript, the CN-480-600 is set to be the key sample and 600 °C should be an appropriate treatment temperature after comprehensive consideration. As a result, only the CN-480 and CN-480-600 were proceeded the XPS measurement in order to study the composition of the samples, especially the situation of reduction of N atoms after heat treatment. Since the sample CN-480-500 is less representative, it has not been tested by SEM and BET.

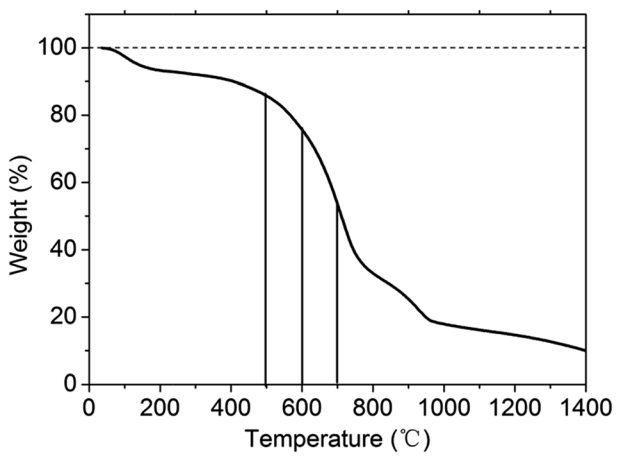

Fig. 4 TGA curves of the sample CN-480.

XPS measurements (Fig. 5) reveal further details of these carbon nitride polymers. Fig. 5(a) shows the XPS survey spectra of the CN-480 and CN-480-600. No peaks of other elements except C, N, and O are observed on the survey spectra which means NaCl have been removed cleanly. The fine spectra are taken in the C1s (Fig. 5(b and d)) and N1s (Fig. 5(c and e)) regions. The C1s spectra can be deconvoluted into two peaks at 284.9 and 286.8 eV. The peak at 284.9 eV reveals the existence of –C≡N[26,27] (may come from the degradation of s-triazine rings) and the peak at 286.8 eV can be assigned to the N–C=N species which is the major carbon species in s-triazine rings.[25,28,29] The N1s spectra can also be fitted into two peaks. The peaks with the lower binding energies, centred at 398.8 eV, can be attributed to the sp^2 nitrogen involved in the s-triazine rings (C–N=C), while the peak with the highest binding energy at 400.6 eV can be assigned to the –C≡N species.[26,27,30] There is no other peak appears at about 399–400 eV which corresponds to the tertiary amine group ($N–(C)_3$), indicating the s-triazine rings are directly interconnected with each other rather than bridged by a N atom. This further confirms that our synthesis have been carried out as the reaction scheme mentioned above.

The distributions of C atoms and N atoms from the XPS analysis are shown in Table 2. It can be seen that the contents of both C atom and N atom decrease after heat treatment, and the

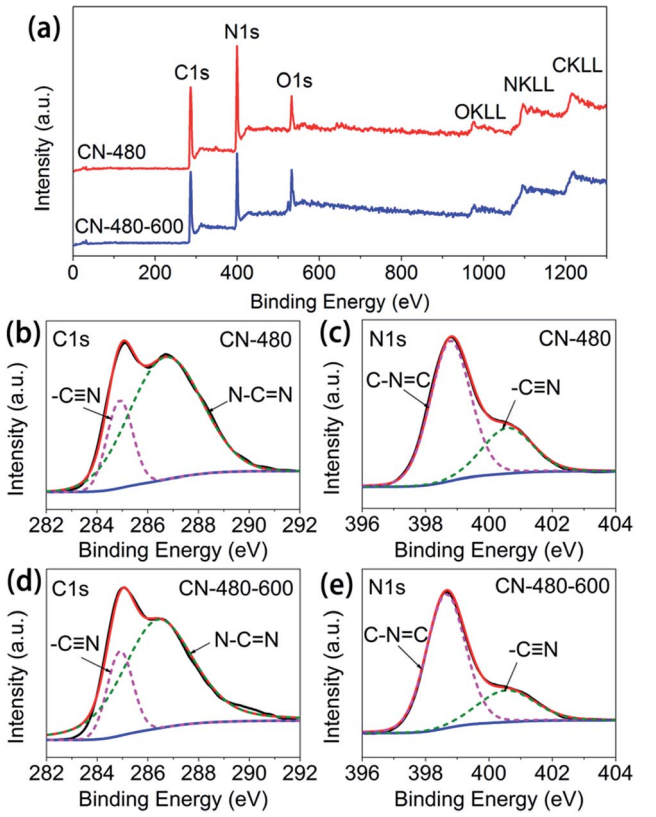

Fig. 5 The XPS spectra of the CN-480 and CN-480-600. (a) Survey spectra. (b, d) C1s region. (c, e) N1s region.

Table 2 Distributions of C atoms and N atoms in the samples before and after heat treatment

Samples		C1s	N1s
CN-480	Peak area	23 283	22 432
CN-480-600	Peak area	21 519	16 461

loss of N atoms is greater than that of C atoms, which is in consistent with the results of bulk elemental analysis.

SEM images of CN-380, CN-480 and CN-480-600 at different magnifications are shown in Fig. 6(a)–(f). It clearly shows that three samples are micro-sized particles with macro porous pores. Among them, Fig. 6(b) and bottom right corner of Fig. 6(c) show the cross section of the macro porous structure. The pieces of the sample CN-380 (Fig. 6(a)) and the sample CN-480 (Fig. 6(c)), due to the grind process, should be come from the rupture of huge macro porous bulks (Fig. 6(b)–(d)), respectively. After heat treatment, a lot of nanodots, which cannot be found in the CN-480, suddenly appear at the edge of the macro porous structure (see Fig. 6(e and f)). These nanodots not only increase the ratio surface area but also provide evidence that small-scaled structural rearrangement happens during the heat treatment.

Fig. 7 shows the BET data and pore distribution data of the three synthesized samples. The specific BET surface areas of sample CN-380, CN-480 and CN-480-600 are as low as 16.7 $m^2 g^{-1}$, 12.0 $m^2 g^{-1}$ and 19.8 $m^2 g^{-1}$, respectively. The lower surface area of CN-480 may be due to the partial pore amalgamation at higher temperature when compared with that of CN-380. From the Fig. 7(b), it can be seen that the pore diameter distribution of CN-380 is mainly concentrated on ~300 nm, while for sample CN-480, the diameter distribution is centred on 500–600 nm.

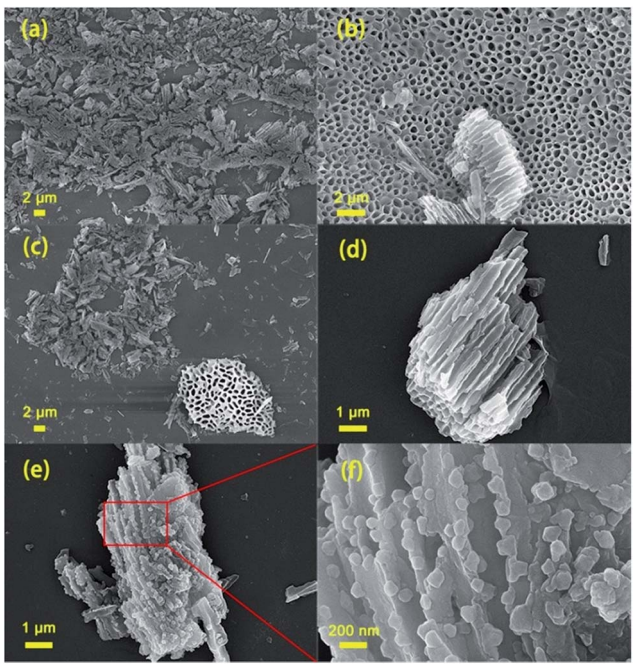

Fig. 6 FE-SEM images of CN-380 (a, b), CN-480 (c, d) and CN-480-600 (e, f) at different magnifications.

This can help support our previous pore amalgamation speculation from another side. The CN-480-600 shows a higher surface area than CN-480 which may result from the decrease of nitrogen content and the partial degradation of triazine rings after heat treatment.

The synthesized samples were further investigated as anode material for lithium half-cells. The typical cyclic voltammograms (CVs) of CN-380, CN-480, CN-480-500 and CN-480-600 are shown in Fig. 8(a, c, e and g), respectively. The CVs containing

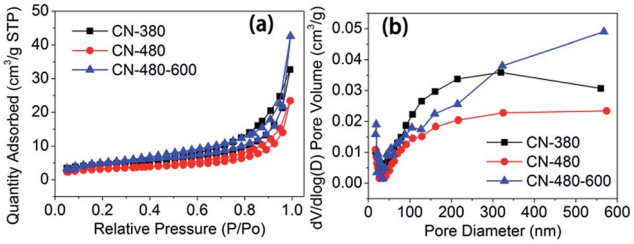

Fig. 7 N_2 adsorption–desorption isotherms (a) and pore size distributions (b) of synthesized samples.

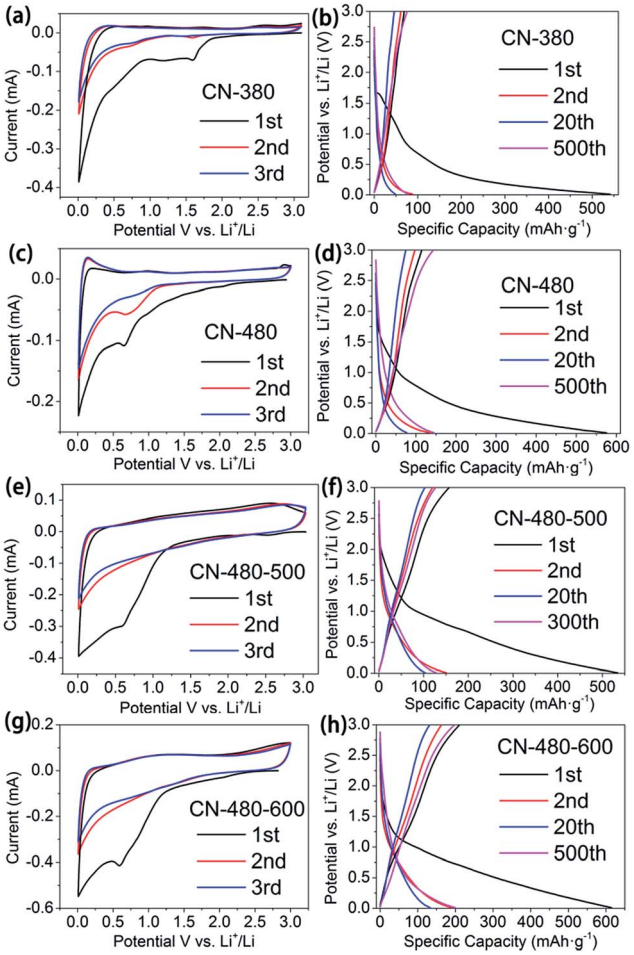

Fig. 8 Electrochemical performances of CN-380, CN-480, CN-480-500 and CN-480-600: CVs of the initial three cycles at a scan rate of 0.2 mV s^{-1} (a, c, e and g); charge–discharge curves at 100 mA g^{-1} (b, d, f and h).

three successive cycles were recorded in the potential range of 0.01–3.0 V *vs.* Li^+/Li. During the first cycle, the irreversible broad cathodic current peak that appears at 1.59 V, 0.65 V, 0.59 V and 0.59 V respectively, can be attributed to the formation of stable SEI, the decomposition of electrolyte, and side reactions.[31,32] On further cycling, the consecutive cyclic voltammograms are very much indistinguishable, indicating the reversibility of intercalation/deintercalation reactions on synthesized samples.

Fig. 8(b, d, f and h) represents the galvanostatic charge/discharge profile of CN-380, CN-480, CN-480-500 and CN-480-600, cycled between 0.01 to 3.0 V at a current density of 100 mA g^{-1}. The voltage profiles of the four samples are similar to previously reported N-doped carbon materials and mesoporous graphene nanosheets.[31–34] The CN-380 anode material delivers a relatively high discharge capacity of about 541.3 mA h g^{-1} at the initial cycle, while its first reversible capacity is only 68.9 mA h g^{-1} with initial coulombic efficiency of only 12.7%. In case of CN-480 anode material, a large irreversible capacity of 575.7 mA h g^{-1} is measured in the first cycle with an initial coulombic efficiency of about 19.9%. The large irreversible capacity could be attributed to the formation of stable SEI and/or to irreversible lithium insertion into special positions and strongly binds with nitrogen in $6C_3N_3$ pores.[16,32,35]

However, the capacity becomes stable and reversible after the first cycle. Surprisingly, the initial coulombic efficiency of CN-480-500 and CN-480-600, though not high enough, increases to 29.5% and 34.3% respectively when compared with CN-480 (see the inset of Fig. 9(a)). This indicates that the heat treatment can help reduce the irreversible capacity which may thank to the decrease of N atoms content and the partial degradation and rearrangement of triazine rings leading to decrease of lithium ion irreversible binding sites. Similarly, the assumption above can be also applied to the sample CN-380 and CN-480 (12.7% and 19.9%, respectively).

The cycling performance of the synthesized samples were evaluated at 100 mA g^{-1} over a range of 0.01–3.0 V. As shown in Fig. 9(a), four samples show good cyclic stability after 500 cycles. As the matter of revision time, the cycling performance of CN-480-500 was evaluated for only 300 cycles but we think it was long enough to compare with other samples. The reversible capacities of four samples reduce quickly in the first 20th cycles and then progressively increase to 75.9 mA h g^{-1}, 143.3 mA h g^{-1}, 127 mA h g^{-1} (300 cycles) and 197.8 mA h g^{-1} respectively, which can be attributed to the activating process of the porous anodes.[6,32] CN-480 anode shows the higher reversible capacity than that of CN-380, due to the more defects in the sample CN-480. And obviously, the heat treatment can also enhance the reversible capacity of CN-480. Although the reversible capacities of four samples are less than that of graphite, it is still superior to that of bulk g-C_3N_4 or other graphite carbon nitrides analogues (the comparison is shown in Table 3).[1,8,36]

To better understand the electrochemical performance of the as-prepared samples, we further studied the rate performance, which are presented in Fig. 9(b). With the increase of charge/discharge current densities from 10 to 1000 mA g^{-1} (the current density in first three cycles is 100 mA g^{-1}), the reversible capacities of the CN-480-600 anode are about 274.4, 74.6, 51.9, 42.5, 31.2 and 23.3 mA h g^{-1} at 10, 50, 100, 200, 500 and 1000 mA g^{-1} successively. When the current density was switched back to 10 mA g^{-1}, the capacity of the CN-480-600

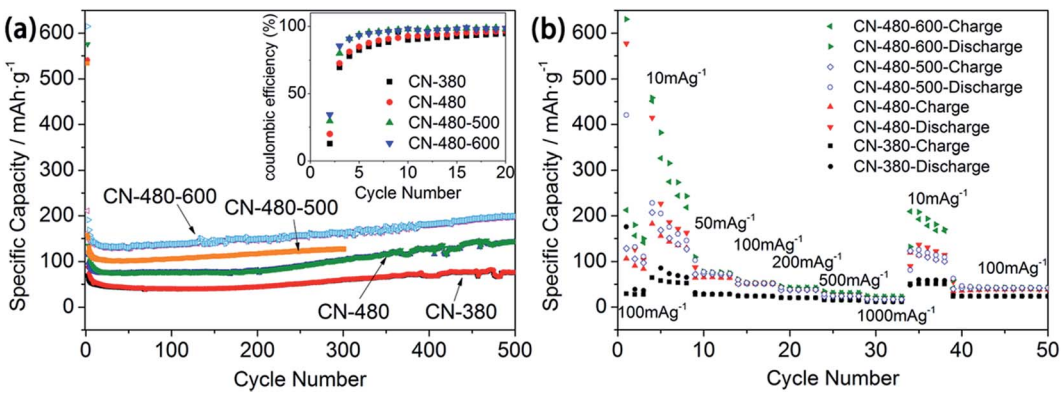

Fig. 9 Cyclability at 100 mA g^{-1} (a) (the inset is the coulombic efficiency of four samples in the first 20 cycles) and comparison of rate performance (b) of CN-380, CN-480, CN-480-500 and CN-480-600.

Table 3 Electrochemical performance of other reported graphite carbon nitrides analogues

Sample	Reversible capacity	Initial coulombic efficiency	Current density	Cycle number	*vs.* Li^+/Li	Ref.
g-C_3N_4	68 mA h g^{-1}	45%	100 mA g^{-1}	2	0.01–3V	1
Disordered C_3N_4	38 mA h g^{-1}	20%	4 μA cm^{-2}	6	0.01–3V	8
gCNMs-550	8 mA h g^{-1}	78%	2 mA g^{-1}	2	0.01–3V	36
CN-480-600	197.8 mA h g^{-1}	34.3%	100 mA g^{-1}	500	0.01–3V	This study

anode reduces to 178.1 mA h g^{-1} which may result from the unsatisfied electronic conductivity. In addition, CN-380, CN-480, and CN-480-500 anode show a similar rate performance with a lower reversible capacity.

4. Conclusion

In summary, we have successfully prepared the macroporous graphite-like C_3N_3 (g-C_3N_3) with s-triazine rings as building blocks by the Wurtz reaction of $C_3N_3Cl_3$ with sodium in autoclaves. As the anode material for Li-ion batteries, four samples show relatively higher reversible capacities when compared with the reported bulk g-C_3N_4 and other graphite carbon nitrides analogues. However, large irreversible capacities are inevitable appeared in the first cycle, which validates the results of Hankel's study. And the electro-chemical performance of the synthesized nitrogen rich carbon material are worse than that of previous reported nitrogen doped carbon material, which is in paradox with the expectation of previous study. Namely, the doping of nitrogen with a relative low ratio can indeed enhance the electrochemical performance. However, more N atoms in the as synthesized samples may cause the irreversible lithium insertion into special positions and strongly binding with nitrogen in 6C_3N_3 pores. Surprisingly, we find that the heat treatment at 600 °C can apparently help improve the initial coulombic efficiency and reversible capacity due to the decrease of N atom content and the partial degradation and rearrangement of triazine rings. Moreover, the CN-480 anode exhibits a superior electrochemical performance in comparison to CN-380 anode. Although the synthesized g-C_3N_3 performs not good enough as anode material in lithium ion battery, we still believe the g-C_3N_3 analogues can be alternative anode materials if further improvements have thoroughly figure out the relative problems. We hope this article could provide a way of thinking and a guide for the further development of alternative anode materials in LIBs.

Conflicts of interest

There are no conflicts to declare.

Acknowledgements

The project is sponsored by the Natural Science Foundation of Fujian Province (No. 2010J05034) and the Scientific Research Foundation for the Returned Overseas Chinese Scholars, State Education Ministry (Batch No. 44).

References

1 Y. Fu, J. Zhu, C. Hu, X. Wu and X. Wang, *Nanoscale*, 2014, **6**, 12555–12564.
2 G. Wu, R. Li, Z. Li, J. Liu, Z. Gu and G. Wang, *Electrochim. Acta*, 2015, **171**, 156–164.
3 Y. Tang, L. Liu, X. Wang, D. Jia, W. Xia, Z. Zhao and J. Qiu, *J. Power Sources*, 2016, **319**, 227–234.
4 H. Lyu, J. Liu, S. Qiu, Y. Cao, C. Hu, S. Guo and Z. Guo, *J. Mater. Chem. A*, 2016, **4**, 9881–9889.
5 Z. Wu, W. Ren, L. Xu, F. Li and H. Cheng, *ACS Nano*, 2011, **5**, 5463–5471.
6 X. W. Liu, Y. Wu, Z. Z. Yang, F. S. Pan, X. W. Zhong, J. Q. Wang, L. Gu and Y. Yu, *J. Power Sources*, 2015, **293**, 799–805.
7 M. Hankel, D. L. Ye, L. Z. Wang and D. J. Searles, *J. Phys. Chem. C*, 2015, **119**, 21921–21927.
8 G. M. Veith, L. Baggetto, L. A. Adamczyk, B. K. Guo, S. S. Brown, X. G. Sun, A. A. Albert, J. R. Humble, C. E. Barnes, M. J. Bojdys, S. Dai and N. J. Dudney, *Chem. Mater.*, 2013, **25**, 503–508.
9 Y. Liu, L. Yu, C. N. Ong and J. Xie, *Nano Res.*, 2016, **9**, 1983–1993.
10 Y. B. Liu, Y. Y. Zheng, B. W. Du, R. R. Nasaruddin, T. Chen and J. P. Xie, *Ind. Eng. Chem. Res.*, 2017, **56**, 2999–3007.
11 J. G. Li, Q. Liu, Y. B. Liu and J. P. Xie, *Environ. Sci.: Water Res. Technol.*, 2017, **3**, 139–146.
12 M. H. Wu, Q. Wang, Q. Sun and P. R. Jena, *J. Phys. Chem. C*, 2013, **117**, 6055–6059.
13 H. H. Qiu, Z. J. Wang and X. L. Sheng, *Phys. Lett. A*, 2013, **377**, 347–350.
14 Q. X. Guo, Q. Yang, C. Q. Yi, L. Zhu and Y. Xie, *Carbon*, 2005, **43**, 1386–1391.
15 H. Li, C. B. Cao, H. W. Hao, H. L. Qiu, Y. J. Xu and H. S. Zhu, *Diamond Relat. Mater.*, 2006, **15**, 1593–1600.
16 M. Hankel and D. J. Searles, *Phys. Chem. Chem. Phys.*, 2016, **18**, 14205–14215.
17 Y. Xu, M. Xie, S. Huang, H. Xu, H. Ji, J. Xia, Y. Li and H. Li, *RSC Adv.*, 2015, **5**, 26281–26290.
18 F. Dong, Z. W. Zhao, T. Xiong, Z. L. Ni, W. D. Zhang, Y. J. Sun and W. K. Ho, *ACS Appl. Mater. Interfaces*, 2013, **5**, 11392–11401.
19 L. Shi, T. Liang, L. Liang, F. X. Wang, M. S. Liu and J. M. Sun, *J. Porous Mater.*, 2015, **22**, 1393–1399.
20 Y. Zhang, H. F. Zhao, Z. J. Hu, H. Chen, X. J. Zhang, Q. Huang, Q. Z. Wo and S. G. Zhang, *Chempluschem*, 2015, **80**, 1139–1147.
21 N. Xiao, D. M. Lau, W. H. Shi, J. X. Zhu, X. C. Dong, H. H. Hng and Q. Y. Yan, *Carbon*, 2013, **57**, 184–190.
22 J. Ma, B. L. Guo, X. T. Cao, Y. P. Lin, B. X. Yao, F. M. Li, W. Weng and L. Z. Huang, *Talanta*, 2015, **143**, 205–211.
23 E. G. Gillan, *Chem. Mater.*, 2000, **12**, 3906–3912.
24 C. Fettkenhauer, J. Weber, M. Antonietti and D. Dontsova, *RSC Adv.*, 2014, **4**, 40803–40811.
25 Y. Cao, Z. Zhang, J. Long, J. Liang, H. Lin, H. Lin and X. Wang, *J. Mater. Chem. A*, 2014, **2**, 17797–17807.
26 C. D. Wagner, W. M. Riggs, L. E. Davis and J. F. Moulder, *Handbook of X-ray photoelectron spectroscopy*, Perkin-Elmer, 1979.
27 C. D. Wagner, A. V. Naumkin and A. Kraut-Vass, *NIST Standard Reference Database*, vol. 20, 2003.
28 J. Xu, K. Shen, B. Xue and Y. Li, *J. Mol. Catal. A: Chem.*, 2013, **372**, 105–113.
29 J. Xu, K. Long, T. Chen, B. Xue, Y. Li and Y. Cao, *Catal. Sci. Technol.*, 2013, **3**, 3192–3199.

30 V. N. Khabashesku, J. L. Zimmerman and J. L. Margrave, *Chem. Mater.*, 2000, **12**, 3264–3270.
31 K. R. Saravanan and N. Kalaiselvi, *Carbon*, 2015, **81**, 43–53.
32 L. Qie, W. Chen, Z. Wang, Q. Shao, X. Li, L. Yuan, X. Hu, W. Zhang and Y. Huang, *Adv. Mater.*, 2012, **24**, 2047–2050.
33 V. Selvamani, R. Ravikumar, V. Suryanarayanan, D. Velayutham and S. Gopukumar, *Electrochim. Acta*, 2015, **182**, 1–10.
34 Y. Fang, Y. Lv, R. Che, H. Wu, X. Zhang, D. Gu, G. Zheng and D. Zhao, *J. Am. Chem. Soc.*, 2013, **135**, 1524–1530.
35 J. Hou, C. Cao, F. Idrees and X. Ma, *ACS Nano*, 2015, **9**, 2556–2564.
36 A. B. Jorge, F. Cora, A. Sella, P. F. McMillan and D. J. L. Brett, *Int. J. Nanotechnol.*, 2014, **11**, 737–746.